Journal of Optics

PAPER

Axiparabola: a new tool for high-intensity optics

To cite this article: Kosta Oubrerie *et al* 2022 *J. Opt.* **24** 045503

View the article online for updates and enhancements.

You may also like

- Cavitation in centrifugal pump with rotating walls of axial inlet device
O Moloshnyi and M Sotnyk
- Capillary Plasma Formation by a Laser
Nitikant and A K Sharma
- A Graphic Method of Optical Imagery
William R Bower

IOP ebooks™

Bringing together innovative digital publishing with leading authors from the global scientific community.

Start exploring the collection–download the first chapter of every title for free.

This content was downloaded from IP address 128.141.191.11 on 24/08/2022 at 14:25

IOP Publishing Journal of Optics
J. Opt. **24** (2022) 045503 (9pp) https://doi.org/10.1088/2040-8986/ac57d2

Axiparabola: a new tool for high-intensity optics

Kosta Oubrerie[1,*], Igor A Andriyash[1], Ronan Lahaye[1], Slava Smartsev[2], Victor Malka[2] and Cédric Thaury[1]

[1] Laboratoire d'Optique Appliquée, École Polytechnique, ENSTA Paris, CNRS, Institut Polytechnique de Paris, 91762 Palaiseau, France
[2] Department of Physics of Complex Systems, Weizmann Institute of Science, Rehovot 7610001, Israel

E-mail: kosta.oubrerie@ensta-paris.fr

Received 18 October 2021, revised 2 February 2022
Accepted for publication 23 February 2022
Published 7 March 2022

Abstract

An axiparabola is a reflective aspherical optics that focuses a light beam into an extended focal line. The light intensity and group velocity profiles along the focus are adjustable through the proper design. The on-axis light velocity can be controlled, for instance, by adding spatio-temporal couplings via chromatic optics on the incoming beam. Therefore the energy deposition along the axis can be either subluminal or superluminal as required in various applications. This article first explores how the axiparabola design defines its properties in the geometric optics approximation. Then the obtained description is considered in numerical simulations for two cases of interest for laser-plasma acceleration. We show that the axiparabola can be used either to generate a plasma waveguide to overcome diffraction or for driving a dephasingless wakefield accelerator.

Keywords: laser, optics, spatio-temporal couplings, longitudinal chromatism/pulse front curvature, laserwakefield acceleration

(Some figures may appear in colour only in the online journal)

1. Introduction

Bessel beams are diffractionless light waves and can propagate with subluminal or superluminal velocities [1]. These properties have found many applications in material processing [2], optical guiding of microscopic particles [3], optical coherence tomography [4] and formation of plasma waveguides [5]. Several optics, e.g. axilenses [6], axicon lenses [7], or conic mirrors, are able to generate quasi-Bessel beams. The axiparabola is an aspherical mirror, which combines the advantages of these different optics by being achromatic, having a high damage threshold and allowing for control of the intensity distribution along the focal line [8]. These features make it the perfect tool for producing ultra-short quasi-Bessel beams at very high intensity.

A beam focused by an axiparabola has phase and group velocities, which are equal to each other, and in vacuum they are larger than the speed of light in vacuum c [9]. Depending on the mirror design, the beam's on-axis velocity can either only grow or only fall along the focal line. Moreover, the intensity and velocity profiles are fully coupled: any change of the optics surface through its so-called *sag function*, aiming at modifying the intensity profile, impacts the velocity profile. However, this restriction changes if the focused beam initially contains spatio-temporal couplings (STC), which allow to decouple the intensity and velocity profiles.

In this article, we study theoretically the properties of a laser beam focused by an axiparabola and we present ways to control these properties by the means of STC. We first derive basic equations and describe the intensity and velocity profiles without STC and in the geometrical optics approximation. Secondly, we explore effects of STC on a velocity profile and determine the way to control it. We then present an

* Author to whom any correspondence should be addressed.

 © 2022 IOP Publishing Ltd

optical propagation algorithm, which we further use to confirm the predictions of geometric optics. Finally we discuss in more detail two examples of axiparabolas of relevance for laser plasma accelerators development, such as dephasingless wakefield acceleration [10–12] or diffractionless wakefield acceleration with an all-optical plasma waveguide [8, 13, 14].

2. Basic equations

An axiparabola is an aspheric mirror that reflects a collimated beam into an extended focal line by focusing rays at different focal planes depending on their radial coordinate r on the mirror. The shape of its surface is defined by the sag function $s(r)$. The rays coming parallel to the optical axis ζ at the radial coordinate r impinge the mirror at $\zeta = s(r)$ and are focused at $\zeta = f(r) = f_0 + z(r)$ with f_0 the nominal focal length, $z(r) \in [0, \delta]$ the focal line coordinate along the ζ axis, and $|\delta|$ the focal depth (see figure 1(a)). The main differences between an axiparabola and an axicon lens, or a conic mirror, is that f_0 is non-zero, and that δ can be either positive or negative ($\delta < 0$ corresponds to outer rays focused first). This means that the focal spot size and effective Rayleigh range are decoupled. The mean focal spot transverse size is controlled by f_0 and the focal range ('effective Rayleigh range') by δ.

From geometrical optics laws, the sag function is defined by [8]:

$$s(r) + \frac{r}{2}\left(\frac{1}{D(r)} - D(r)\right) = f(r), \tag{1}$$

with $D(r) = ds/dr$ the sag derivative with respect to the radial coordinate. Computing $D(r)$ and choosing the positive solution, we get:

$$r\frac{ds}{dr} = s(r) - f(r) + \sqrt{[s(r) - f(r)]^2 + r^2}. \tag{2}$$

Let $\sigma(r) = s(r) - r^2/4f_0$ be the deviation to a perfect parabola and R the beam radius. Assuming that the deviation to a parabola is small, $\sigma \ll r^2/4f_0$ and $\delta^2/8R^2 \ll 1$, equation (2) can be approximated as:

$$\frac{d\sigma(r)}{dr} = -\frac{rz(r)}{2ff_0} + o(r^3). \tag{3}$$

The integration of equation (2) or (3) allows to determine the required sag function for achieving a given focal line $f(r)$. This will fix the intensity distribution at focus as well as the light velocity evolution along the focal line.

2.1. Longitudinal intensity distribution

A key parameter for the practical use of axiparabolas is the intensity distribution along the propagation axis. Let us start from the geometrical optics description and define $\lambda_z(z)$ as the linear density of ray along the propagation axis ζ (in W.m^{-1}). The laser intensity on the axiparabola $I_0(r)$ (in W.m^{-2}) is defined as the surface density of rays, and it is related to the linear ray density as [15]:

$$\lambda_z(z)dz = 2\,\pi r dr I_0(r). \tag{4}$$

In the present study we assume a top-hat beam profile, so that the intensity on the mirror is uniform, $I_0(r) = P_0/(\pi R^2)$ with P_0 the incident power, leading to:

$$\frac{dr}{dz} = \frac{\lambda_z(z)R^2}{2P_0\, r}, \tag{5}$$

and finally

$$r(z) = R\left(\int_0^z \frac{\lambda_z(z')}{P_0}dz'\right)^{1/2}. \tag{6}$$

This equation allows to calculate the function $r(z)$ and hence the sag function defining the desired intensity profile $\lambda_z(z)$ [16]. For instance, for a focal line of constant intensity, $\lambda_z = P_0/\delta$, we get that $f = f_0 + \delta r^2/R^2$. The sag function can then be obtained by integration of equation (2).

2.2. Transverse intensity distribution

While for a classical focusing optic, the focal depth, or in other words the Rayleigh length, is closely linked to the beam waist, these two quantities are decoupled at the focus of an axiparabola. For the sake of simplicity, we illustrate this property by considering a top-hat incident beam. In the Fresnel diffraction regime, the field at the distance $f(r) = f_0 + z(r)$ from the axiparabola is:

$$E(r_\zeta, z) = -i\frac{E_0\, k}{f(r)}\, e^{ik\left(f(r) + \frac{r_\zeta^2}{2f(r)}\right)} \int_0^R dr e^{i\Psi(r)} r J_0\left(k\frac{r_\zeta r}{f(r)}\right), \tag{7}$$

with $k = 2\pi/\lambda$ the wave-vector, r_ζ the radial coordinate over the focal line, J_0 the first Bessel function of first kind and:

$$\Psi(x) = k\left(x^2/2f(x) - 2s(x)\right) = k\left(x^2/2f(x) - x^2/2f_0 - 2\sigma(x)\right),$$

for $z \ll f_0$. For $r \gg 1/k$ we can use the stationary phase method to estimate the integral [17, 18]:

$$E(r_\zeta, z) = -i\frac{E_0\, k}{f(r)} e^{ik\left(f(r) + \frac{r_\zeta^2}{2f(r)}\right)} \sqrt{\frac{2\pi}{\Psi''(r_s)}} r_s J_0 \times \left(k\frac{r_\zeta r_s}{f(r)}\right) e^{i\Psi(r_s) + i\pi/4}, \tag{8}$$

with r_s the coordinate such as $\Psi'(r_s) = 0$ (note that we assumed $\Psi''(r_s) > 0$). According to equation (3), we have:

$$\Psi'(x) \approx -k\frac{xz(x)}{ff_0} + k\frac{xz(x)}{ff_0} + o\left(kx^3/f_0^2\right).$$

It follows from equation (5) that $\Psi''(r_s) = 2\, r_s^2 P_0/(\lambda_z(z)\, R^2\, f_0^2)$. As a consequence, the intensity along the focal line is:

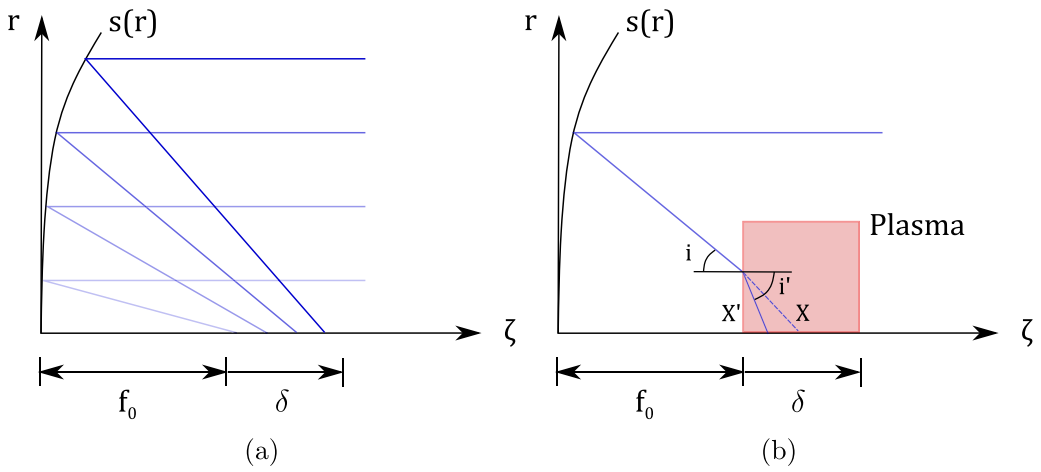

Figure 1. (a) Schematic representation of rays focused by an axiparabola with a positive δ. (b) Schematic representation of a ray focused by an axiparabola with a positive δ in a constant density plasma.

$$I(r_\zeta,z) = |E(r_\zeta,z)|^2 = \frac{E_0^2k^2}{f_0^2}\frac{2\pi}{k\Psi''(r_s)}r_s^2\,J_0^2\left(k\frac{r_\zeta r_s}{f_0}\right) = k\lambda_z(z)J_0^2\left(k\frac{r_\zeta r_s}{f_0}\right), \tag{9}$$

with

$$r_s = R\sqrt{\int_0^z \frac{\lambda_z(z')}{P_0}dz'}. \tag{10}$$

One may easily see that the radial intensity profile is described by the first Bessel function and that the on-axis intensity is $I_0(z) = I(0,z) = k\lambda_z(z)$. We finally find that the first-zero radius, for $r_s \gg 1/k$, is:

$$r_{\zeta,0}(z) \approx 0.77\,\lambda N\left(\int_0^z \frac{I_0(z')}{kP_0}dz'\right)^{-1/2}, \tag{11}$$

with $N = f_0/2\,R$ the f-number. As a result, equations (9) and (11) show that the intensity does not depend on N, and hence that r_0 can be adjusted independently of I_0 by changing N. For example, for a constant intensity focal line we get $I_0 = kP_0/\delta$ and $r_{\zeta,0} = 0.77\lambda N(\delta/z)^{1/2}$; the intensity at focus depends only on the beam power and focal depth, while the focal spot is a function of N. Therefore an axiparabola can redistribute the laser energy into a focal line combining a long focal depth and a very small focal spot.

2.3. Velocity profile

It is well-known that Bessel beams travel at constant velocities that can exceed light speed in vacuum. However, as shown in previous section, an axiparabola generates a quasi-Bessel beam, for which the longitudinal group velocity is still superluminal but is no longer constant. Defining the group velocity of the beam as the velocity of the intensity peak along the focal line we can describe it using equation (2). The optical path of light in vacuum from a certain plane perpendicular to the optical axis and reflecting on the axiparabola to the optical axis is:

$$p(r) = \sqrt{[s(r)-f(r)]^2 + r^2} - s(r). \tag{12}$$

The geometrical group velocity is the change of the focus position in time $v = df/dt$, and we note that the increase of the optical path on axis ζ is $dp = cdt$. With that in mind, we can parametrize differentials as functions of r, and express the group velocity as:

$$\frac{v}{c} = \frac{df}{dr}\left(\frac{dp}{dr}\right)^{-1} = \left(\frac{dp}{dz}\right)^{-1}. \tag{13}$$

Then using equations (2) and (12), we get in the paraxial limit:

$$\frac{v}{c} = 1 + \frac{2\left(\frac{ds}{dr}\right)^2}{1-\left(\frac{ds}{dr}\right)^2} = 1 + \frac{r^2}{2f^2}. \tag{14}$$

Equation (14) shows that the group velocity is always larger than the speed of light in vacuum [19, 20] and that its evolution along the focal line can be either increasing or decreasing, depending on whether δ is positive or negative respectively. For a top-hat incident beam, we get from equation (6) that the group velocity of the focal line is:

$$\frac{v}{c} = 1 + \frac{R^2}{2f^2P_0}\int_0^z \lambda_z(z')dz', \tag{15}$$

which illustrates the direct relation of the group velocity to the local intensity. This link between velocity and intensity hinders the actual ability of axiparabolas to control the velocity of laser power propagation. Nevertheless, as will be shown later, this scheme still holds the opportunity to dissociate that connection through STC, which gives another degree of freedom to control and modify the group velocity along the focal line.

3. Control of the velocity

3.1. Group velocity

Axiparabola focuses different annular beamlets annuli to different focal planes depending on their incident radial coordinates. This spatial separation allows for control of the beamlets arrival and thus control of the group velocity [21]. In other words: group velocity along the focal line depends on the radial coordinate on the mirror. Hence, its value can be modified by adding a radial delay prior to the axiparabola. This can be exemplified by considering a linear propagation in vacuum. Starting from equation (13), a radial delay $\tau(r)$ is added and modifies the velocity υ as υ_m:

$$\frac{\upsilon_m}{c} = \left(\frac{d(p+c\tau)}{dz'}\right)^{-1}. \tag{16}$$

Assuming that $p \gg c\tau$, this leads to:

$$\frac{\upsilon_m}{c} \simeq \frac{\upsilon}{c}\left(1 - \frac{\upsilon}{c} c \frac{d\tau}{dr}\frac{dr}{dz}\right). \tag{17}$$

This highlights that the velocity can be controlled by introducing simple STC. To properly illustrate this phenomenon, let us assume a top-hat beam in the paraxial limit for an axiparabola such as $r^2/2f^2 \ll 1$: the radial delay needed for having an intensity peak that propagates, at a constant velocity $c + \upsilon_0$ with $\upsilon_0 \ll c$, is:

$$c\frac{d\tau}{dr} \simeq \left(\frac{\upsilon}{c} - \frac{\upsilon_0}{c} - 1\right)\left(\frac{c}{\upsilon}\right)^2 \frac{2P_0 r}{\lambda_z R^2}, \tag{18}$$

leading to:

$$c\tau \simeq \frac{P_0}{\lambda_z R^2}\left(-\frac{\upsilon_0}{c}r^2 + \frac{1}{2f^2}\left(\frac{\upsilon_0}{c} + \frac{1}{2}\right)r^4\right) + o(r^5). \tag{19}$$

Here the term $\propto r^4$ flattens the velocity profile to get an intensity peak that propagates at a constant velocity c, while the quadratic term allows to adjust the value of the velocity around c. This quadratic term corresponds to the pulse front curvature (also known as longitudinal chromatic aberration), an aberration which is present in many laser chains, and which can be controlled by using simple plano-convex optics in the laser chain [22, 23]. Achieving the r^4 term would require the use of aspheric lenses, specially designed for a given axiparabola.

This simple prediction model can also be adjusted to take into account the medium in which the laser propagation occurs depending on the applications. For applications in the field of laser-plasma acceleration, the design has also to account for the laser propagation in plasma. For this, let us consider a uniform plasma slab localized in between the focal line's boundaries, i.e. plasma density n_e is constant for $f_0 \leq z \leq f_0 + \delta$ and zero elsewhere, as shown in figure 1(b). The plasma is assumed to be underdense, which means $n_e \ll n_c$, with $n_c = \pi/\left(\lambda_0^2\, r_e\right) = 1.1 \cdot 10^{21}\,(\lambda_0[\mu\mathrm{m}])^{-2}$ cm^{-3} being the critical plasma density for the wavelength λ_0 and r_e the classical electron radius.

Propagation of light in plasma is affected by the refraction at the vacuum/plasma interface and by the modification of the light velocity in plasma. Let $i(r)$ be the angle between the optical axis and the rays that are focused at $z(r)$ in vacuum and $X(r)$ the propagation distance after the vacuum/plasma interface of the rays that are focused at $z(r)$ in vacuum. Assuming paraxial rays, these two variables are defined by:

$$i(r) = \arctan(r/(f-s)), \tag{20}$$

$$z = X\cos(i). \tag{21}$$

The rays that are focused at $z(r)$ in vacuum cross the optical axis at a new coordinate:

$$\begin{aligned} z' &= X'\cos(i') \\ &\simeq z\eta\left(1 + \frac{i^2}{2}\right), \end{aligned} \tag{22}$$

for $i \ll 1$ and with $\eta \simeq 1 - n_e/(2n_c)$ being the refractive index of plasma. This involves a shortening of the focal line ($\delta' < \delta$) that leads to a corresponding increase of the intensity. As the optical path in plasma remains equal to the one in vacuum ($X = X'/\eta$), the decrease of the propagation distance is compensated by the slower group velocity of light in plasma ($\upsilon_g/c = 1 - n_e/(2n_c)$). The group velocity of the focal line in plasma can therefore be written:

$$\upsilon_p = \upsilon\frac{dz'}{dz}, \tag{23}$$

with υ_p the group velocity in plasma and υ the one in vacuum. Following the same method as in equation (17), this involves that the modified velocity in plasma can be written:

$$\frac{\upsilon_{p,m}}{c} \simeq \frac{\upsilon_p}{c}\left(1 - \frac{\upsilon}{c} c \frac{d\tau}{dr}\frac{dr}{dz}\right). \tag{24}$$

From this equation, the required radial delay can be computed with the same process as in equation (18). This study of the group velocity is applicable in vacuum and in any transparent medium and shows that the group velocity can be adjusted independently of the intensity of the focal line, allowing for subluminal or superluminal velocities.

3.2. Phase velocity

In dispersive media, group velocity and phase velocity can be different. Therefore, to fully describe the focal line propagation, the impact of the control of the group velocity through STC on the phase velocity is also of interest. Let $\varphi(z,t) = kp(z) - \omega t$ be the beam phase, with ω the laser pulsation. The phase velocity is:

$$\upsilon_\varphi = \frac{d\varphi/dt}{d\varphi/dz}, \tag{25}$$

and in a plasma and in the absence of STC, its spatial derivative can be written:

$$\frac{d\varphi}{dz} = k\frac{dp}{dz} = \frac{\omega}{\upsilon} \tag{26}$$

with υ the group velocity. This leads to the following formula:

$$\frac{\upsilon_\varphi}{c} = \frac{\upsilon}{c} = 1 + \frac{r^2}{2f^2}. \tag{27}$$

The phase velocity of the focal line is thus equal to its group velocity. Now let us observe the evolution of the phase velocity when a radial delay $\tau(r)$ is added prior to the axiparabola as presented in the previous subsection. The phase is then changed to:

$$\begin{aligned}\varphi_m &= k\,(p + c\tau) - \omega\,(t + \tau)\\ &= kp - \omega t = \varphi.\end{aligned} \tag{28}$$

This means that the focal line phase is not modified by the introduction of a radial delay and therefore the phase velocity is always equal to the unaltered group velocity, and thus different from the group velocity in presence of STC:

$$\frac{\upsilon_\varphi}{c} = \frac{\upsilon}{c} = 1 + \frac{r^2}{2f^2}. \tag{29}$$

4. Optical propagation modeling

To simulate the evolution of the laser field along its path we solve numerically the Helmholtz equation. In the Fourier space, propagation of the complex field $\psi(\omega, k_x, k_y, z)$ from the plane z_0 to z_1 can be computed by multiplying it by the propagator:

$$\psi_1 = \psi_0 \exp\left(i(z_1 - z_0)\sqrt{\omega^2/c^2 - k_x^2 - k_y^2}\right).$$

Here, the field is considered strictly cylindrically symmetric, and solutions can be expressed via cylindric modes, i.e. Bessel functions $\psi(r) = \int r\mathrm{d}r\hat{\psi}J_0(k_r r)$, where k_r is equivalent to $\sqrt{k_x^2 + k_y^2}$ in the propagator expression.

One method, based on the quasi-discrete Hankel transform was demonstrated in [24]. The approach was based on the symmetric transform (same matrix for forward and inverse projections), where both spatial and spectral axes, r and k_r, were built on the zeros of J_0. In the case of a sharply focused beam, the beam waist can be $10^2 - 10^3$ times smaller than the spot on the mirror, and to resolve both one may require large numbers of points along the radial and spectral axes $N_r = N_{k_r} \geq 10^4$.

For our calculations, we have used a non-symmetric transform with different sampling of the initial and focused images. For this we consider field decomposition into the series, $\psi(r_i) = \sum_{j=0}^{N_r-1}\hat{\psi}_j J_0(k_{r,j} r_i)$, where $r_i = R_{\max}\alpha_i/\alpha_{N_r}$ and $k_{r,j} = \alpha_j/R_{\max}$ with α_i defined as the roots of Bessel function J_0 (see [24]). This gives the inverse Hankel transform matrix $T_{ji}^{(-1)} = J_0(\alpha_i\alpha_j/\alpha_{N_r})$, and the forward transform T_{ij}, which is found by the numerical inversion of $T_{ji}^{(-1)}$. To reconstruct the field, we use the re-sampled inverse transform $\overline{T^{(-1)}}_{ji} = J(r_i' k_{r,j})$, where axis $k_{r,j}$ is same as in T_{ij}, but r_i' is sampled uniformly in a small area around the beam effective waist.

Both schemes have been tested numerically in all relevant cases. The resampling scheme demonstrated a very good agreement with the original approach [24] with significant sampling reduction (reduction ~ 8 times of N_r). The implementation of this and a few other schemes can be found in the open-source library '`Axiprop`' in [25].

5. Axiparabola with a constant intensity focal line

Let us now consider an axiparabola design for relevant applications in laser-plasma acceleration. In laser wakefield accelerators (LPA), an ultra-short laser pulse is focused in a plasma to generate a plasma wave. The amplitude of the longitudinal electric field of such a wave can be a few orders of magnitude higher than those created in conventional linear accelerators. One fundamental limitation of LPA is the particle-wave dephasing that is due to the mismatch between the group velocity of the laser in plasma and the velocity of relativistic electrons. A laser pulse focused by an axiparabola to a constant intensity line could be used to drive a plasma wave with a phase velocity equal to the vacuum speed of light, overcoming this limit. As shown in equation (18), the combination of axiparabola and appropriate STC allows to control the group velocity, and hence eventually to phase-lock the light beam velocity on the electron beam velocity. This paved the way for a new acceleration concept that could increase the energy of the generated electrons by at least an order of magnitude [10, 11].

To design an axiparabola with a constant intensity focal line, it was assumed that the linear density of rays $\lambda_z = P_0/\delta$, with δ the focal line length. By replacing the expression of λ_z in equation (6), the focal length expression becomes:

$$f = f_0 + \delta\left(\frac{r}{R}\right)^2 \tag{30}$$

From equation (15), the group velocity can now be written:

$$\frac{\upsilon}{c} = 1 + \frac{R^2}{2\delta f^2}z. \tag{31}$$

Note that the group velocity with this particular axiparabola design has a linear dependence on the position along focal line z. For simulations, the following characteristics were chosen: a nominal focus $f_0 = 400$ mm, a focal line length $\delta = 15$ mm and a radius $R = 38.1$ mm.

In figure 2(a), we plot the radial distribution of laser field intensity mapped along its propagation, and figure 2(b) shows the beam characteristics. From figure 2(b) one can see that, in agreement with theoretical considerations laser intensity remains constant along the focal line. The sinusoidal variations are typical characteristics of a Bessel beam. As the first-zero radius diminishes along the focal line, while the intensity remains constant, the energy encircled in the focal spot also diminishes proportionally to the first-zero radius.

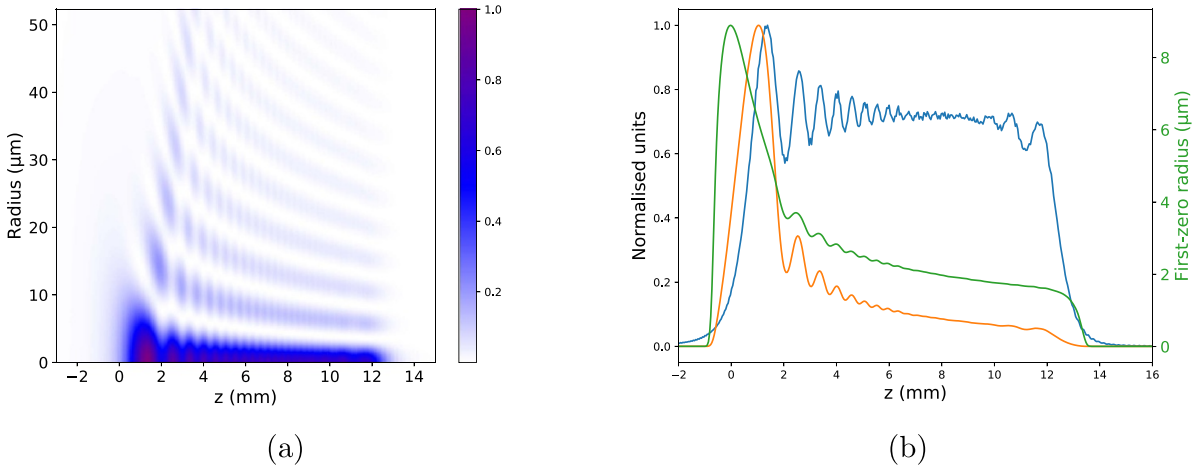

Figure 2. (a) Fluence map of a constant intensity focal line in arbitrary units, as a function of (r, z). (b) Axiparabola relative intensity (blue curve), relative energy which is defined by integrating the intensity in the first-zero radius (orange curve) and first-zero radius (green curve) along the focal line.

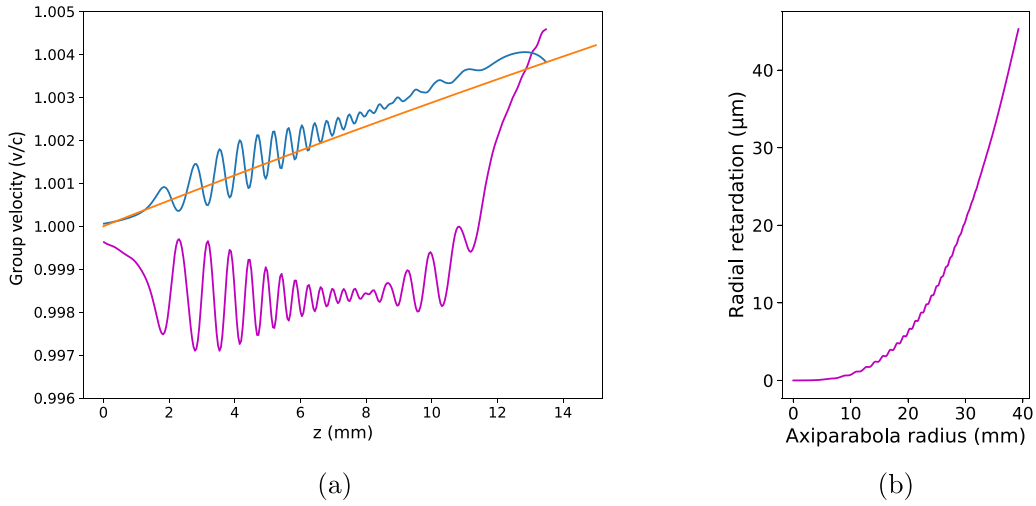

Figure 3. (a) Group velocity as a function of the position along the focal line of the axiparabola. The orange curve corresponds to equation (31), the blue and purple ones to simulation data obtained without and with the radial delay displayed in (b), respectively. (b) Radial delay needed for a group velocity equal to (c), from equation (18).

The group velocity of the focal line is calculated by averaging over the intensity map, hence oscillations are visible within the group velocity's evolution along the focal line (figure 3(a)). Leaving aside the oscillations, which can not be described in the framework of geometrical optics, the group velocity increases linearly with z, as expected from equation (31). The STC computed from equation (18) and shown in figure 3(b), enable to obtain a focal line with a constant group velocity close to the light velocity in vacuum c. The gap observed between the obtained and aimed group velocities, as well as the slope deviation between the orange and blue curves are likely due to the paraxial approximation made to compute the theoretical velocities. The quadratic term of STC should, therefore, be adjusted to get the requested velocity. Note that the end of the focal line also disturbs the measurement of the group velocity, which results in its sudden increase (purple curve in figure 3(a)).

6. Axiparabola with a constant energy focal line

The great versatility of axiparabolas for applications provides the possibility to achieve various focal line distributions. Axiparabolas with various intensity distributions are of particular interest for the investigation of plasma channels generation for guiding purposes (figure 4). The study of an axiparabola with another sag function also allows us to assess the validity and solidity of our theoretical model.

Let's take the example of an axiparabola with a constant energy focal line. In order to obtain a focal line with a constant energy encircled in the central spot, the linear density of rays λ_z needs to compensate for the first-zero radius decrease, as illustrated in figure 2(b). Therefore, following equation (11), λ_z needs to be proportional to the square of the incident rays radius on the axiparabola r : $\lambda_z \propto (r/R)^2$, which leads for a holed axiparabola to

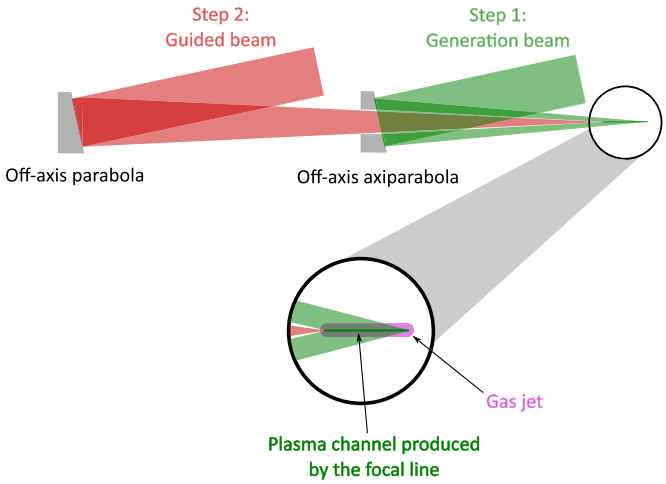

Figure 4. Example of setup for a guiding experiment. The generation beam is focused by an axiparabola and shot a few nanoseconds before the guided beam to allow the formation of the waveguide [8].

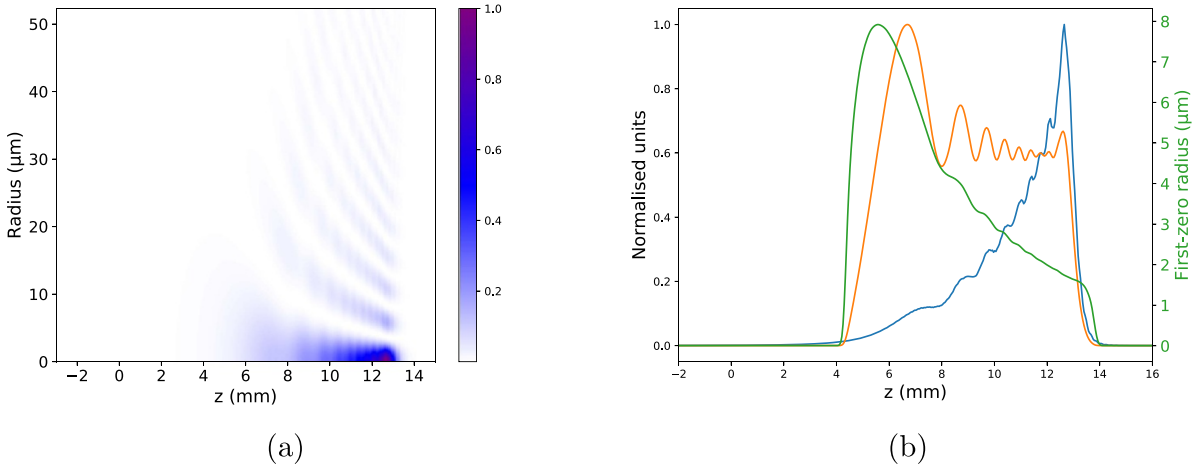

Figure 5. (a) Fluence map of a constant energy focal line in arbitrary units as a function of (r, z). (b) Axiparabola relative intensity (blue curve), relative energy which is defined by integrating the intensity in the first-zero radius (orange curve) and first-zero radius (green curve) along the focal line.

$$f = f_0 + \frac{1}{a}\ln\left(\frac{r}{R}e^{a\delta}\right), \tag{32}$$

with $a = \frac{1}{\delta}\ln\left(\frac{R}{r_{hole}}\right)$ where r_{hole} is the radius of the hole at the center of the axiparabola. However, this simple model overestimates the energy for small radii, which would result in an increasing energy focal line. Therefore, we use an empirical formula similar to the previous one but more in adequation with reality for smaller radii.

In practice this condition is fulfilled for:

$$f = f_0 + 0.1\delta\frac{r}{R} + 0.9\delta\left(\frac{r}{R}\right)^{\frac{1}{2}}, \tag{33}$$

leading to an expression for the group velocity:

$$\frac{v}{c} = 1 + \frac{\delta^2}{f^2}\left(0.405\frac{r}{R} + 0.135\left(\frac{r}{R}\right)^{\frac{3}{2}} + 0.01\left(\frac{r}{R}\right)^2\right). \tag{34}$$

The coefficients of equation (33) were obtained and adjusted through iterations using the propagation code, detailed in section 4, in order to obtain a constant energy focal line.

For simulations, we assume the same parameters as in section 5: a nominal focus $f_0 = 400$ mm, a focal depth $\delta = 15$ mm and a radius $R = 38.1$ mm.

We observe in figure 5(b) that the intensity effectively increases along the focal line to compensate for the decrease of the first-zero radius.

In figure 6, the theoretical group velocity matches the numerical estimate, with the deviation at the end of the focal line, which is mainly due to the ray approximation assumption made to derive equations. This confirms the reliability of the simple model exposed in the first three sections, for axiparabolas with different sag functions and different purposes. The STC needed to obtain a focal line group velocity equal to c is also validated by simulation data.

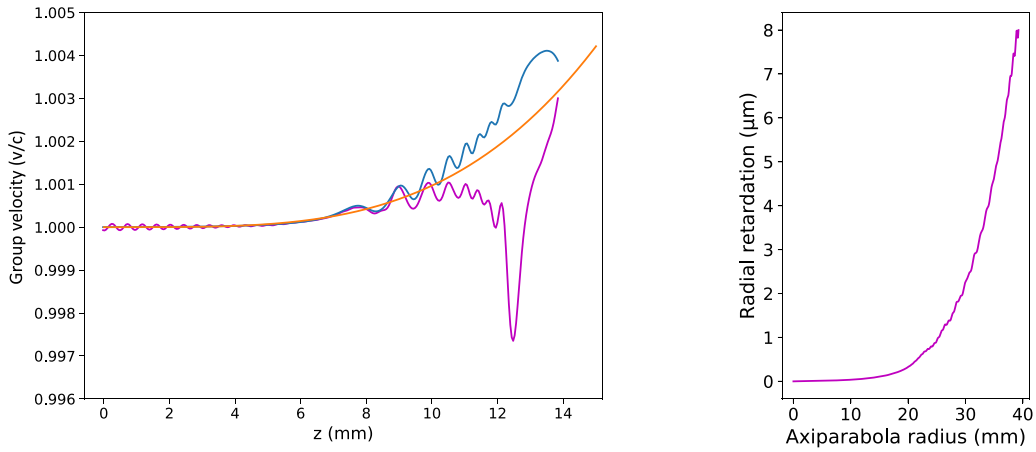

Figure 6. (a) Group velocity as a function of the position along the focal line of the axiparabola. The orange curve results from equation (31). The blue and purple curves correspond to simulation data obtained without and with the radial delay displayed in (b), respectively. (b) Pulse front delay required for the group velocity to equal c, according to equation (18).

7. Conclusion and future work

In conclusion, we demonstrated the possibility to control the longitudinal intensity distribution and the beam velocity, over a distance much larger than the Rayleigh length, using an axiparabola. The adaptability of this aspheric mirror was illustrated by designing and presenting two optical configurations for different applications. We also showed through theory and simulations that the group velocity of the focal line can be controlled through STC and that the corresponding delay can be evaluated from the main axiparabola features. The unique capabilities and versatility of axiparabolas open up new perspectives for manipulating intense and ultra-short laser pulse, which is a promising boost for the development of compact and flexible bright radiation and particles sources in laser wakefield acceleration frame. Moreover, a better control of these high intensity focal line properties (intensity distribution, propagation velocity) can also be an advantage for many other applications, e.g. soft x-ray laser [26], pulse compression in a plasma [27] or photon acceleration [28, 29].

Data availability statement

The data generated and/or analysed during the current study are not publicly available for legal/ethical reasons but are available from the corresponding author on reasonable request.

Acknowledgments

This project has received funding from the European Union's Horizon 2020 Research and Innovation programme under Grant Agreement No. 101004730 LASERLAB-Europe, 730871 ARIES, and 871124 iFAST. We also acknowledge support from the French Agence Nationale de la Recherche (ANR) under reference ANR-19-TERC-0001-01 (TGV project).

ORCID iDs

Kosta Oubrerie https://orcid.org/0000-0002-6676-6856
Igor A Andriyash https://orcid.org/0000-0003-0313-4496
Victor Malka https://orcid.org/0000-0002-0488-2587
Cédric Thaury https://orcid.org/0000-0002-6537-8392

References

[1] Kuntz K, Braverman B, Youn S, Lobino M, Pessina E and Lvovsky A 2009 Spatial and temporal characterization of a Bessel beam produced using a conical mirror *Phys. Rev.* A **79** 043802
[2] Meyer R, Jacquot M, Giust R, Safioui J, Rapp L, Furfaro L, Lacourt P-A, Dudley J M and Courvoisier F 2017 Single-shot ultrafast laser processing of high-aspect-ratio nanochannels using elliptical Bessel beams *Opt. Lett.* **42** 4307–10
[3] Ahlawat S, Verma R S, Dasgupta R and Gupta P K 2011 Long-distance optical guiding of colloidal particles using holographic axilens *Appl. Opt.* **50** 1933–40
[4] Ding Z, Ren H, Zhao Y, Nelson J S and Chen Z 2002 High-resolution optical coherence tomography over a large depth range with an axicon lens *Opt. Lett.* **27** 243–5
[5] Durfee III C and Milchberg H 1993 Light pipe for high intensity laser pulses *Phys. Rev. Lett.* **71** 2409
[6] Davidson N, Friesem A and Hasman E 1991 Holographic axilens: high resolution and long focal depth *Opt. Lett.* **16** 523–5
[7] Arlt J and Dholakia K 2000 Generation of high-order bessel beams by use of an axicon *Opt. Commun.* **177** 297–301
[8] Smartsev S, Caizergues C, Oubrerie K, Gautier J, Goddet J-P, Tafzi A, Phuoc K T, Malka V and Thaury C 2019 Axiparabola: a long-focal-depth, high-resolution mirror for broadband high-intensity lasers *Opt. Lett.* **44** 3414–17
[9] Hernández-Figueroa H E, Zamboni-Rached M and Recami E 2008 *Localized Waves* vol 194 (New York: Wiley)

[10] Caizergues C, Smartsev S, Malka V and Thaury C 2020 Phase-locked laser-wakefield electron acceleration *Nat. Photon.* **14** 475–9
[11] Palastro J, Shaw J, Franke P, Ramsey D, Simpson T and Froula D 2020 Dephasingless laser wakefield acceleration *Phys. Rev. Lett.* **124** 134802
[12] Debus A, Pausch R, Huebl A, Steiniger K, Widera R, Cowan T E, Schramm U and Bussmann M 2019 Circumventing the dephasing and depletion limits of laser-wakefield acceleration *Phys. Rev.* X **9** 031044
[13] Shalloo R, Arran C, Corner L, Holloway J, Jonnerby J, Walczak R, Milchberg H and Hooker S 2018 Hydrodynamic optical-field-ionized plasma channels *Phys. Rev.* E **97** 053203
[14] Shalloo R *et al* 2019 Low-density hydrodynamic optical-field-ionized plasma channels generated with an axicon lens *Phys. Rev. Accel. Beams* **22** 041302
[15] Sochacki J, Kołodziejczyk A, Jaroszewicz Z and Bara S 1992 Nonparaxial design of generalized axicons *Appl. Opt.* **31** 5326–30
[16] Golub I, Chebbi B, Shaw D and Nowacki D 2010 Characterization of a refractive logarithmic axicon *Opt. Lett.* **35** 2828–30
[17] Jaroszewicz Z, Dopazo J R and Gomez-Reino C 1996 Uniformization of the axial intensity of diffraction axicons by polychromatic illumination *Appl. Opt.* **35** 1025–31
[18] Friberg A T 1996 Stationary-phase analysis of generalized axicons *J. Opt. Soc. Am.* A **13** 743–50
[19] Rodrigues W, Thober D S and Xavier Jr A L 2001 Causal explanation for observed superluminal behavior of microwave propagation in free space *Phys. Lett.* A **284** 217–24
[20] Recami E 2001 Superluminal motions? A bird's-eye view of the experimental situation *Found. Phys.* **31** 1119–35
[21] Sainte-Marie A, Gobert O and Quere F 2017 Controlling the velocity of ultrashort light pulses in vacuum through spatio-temporal couplings *Optica* **4** 1298–304
[22] Cui Z *et al* 2019 Dynamic chromatic aberration pre-compensation scheme for ultrashort petawatt laser systems *Opt. Express* **27** 16812–22
[23] Kabacinski A *et al* 2021 Measurement and control of main spatio-temporal couplings in a CPA laser chain *J. Opt.* **23** 06LT01
[24] Guizar-Sicairos M and Gutierrez-Vega J 2004 Computation of quasi-discrete Hankel transforms of integer order for propagating optical wave fields *J. Opt. Soc. Am.* A **21** 53
[25] Andriyash I A 2020 Axiprop: simple-to-use optical propagation tool (available at: https://github.com/hightower8083/axiprop)
[26] Depresseux A *et al* 2015 Table-top femtosecond soft x-ray laser by collisional ionization gating *Nat. Photon.* **9** 817–21
[27] Faure J, Glinec Y, Santos J, Ewald F, Rousseau J-P, Kiselev S, Pukhov A, Hosokai T and Malka V 2005 Observation of laser-pulse shortening in nonlinear plasma waves *Phys. Rev. Lett.* **95** 205003
[28] Wilks S, Dawson J, Mori W, Katsouleas T and Jones M 1989 Photon accelerator *Phys. Rev. Lett.* **62** 2600
[29] Howard A, Turnbull D, Davies A, Franke P, Froula D and Palastro J 2019 Photon acceleration in a flying focus *Phys. Rev. Lett.* **123** 124801